Engineering Structures 243 (2021) 112681

Contents lists available at ScienceDirect

Engineering Structures

journal homepage: www.elsevier.com/locate/engstruct

Seismic performance of an industrial multi-storey frame structure with process equipment subjected to shake table testing

Christoph Butenweg [a], Oreste S. Bursi [b,*], Fabrizio Paolacci [c], Marko Marinković [d], Igor Lanese [e], Chiara Nardin [b], Gianluca Quinci [c]

[a] RWTH-Aachen University, Center for Wind and Earthquake Engineering (CWE), Aachen, Germany
[b] Department of Civil, Environmental and Mechanical Engineering, University of Trento, Via Mesiano 77, 38123 Trento, Italy
[c] Department of Engineering, Roma Tre University, Via Vito Volterra 62, 00146 Rome, Italy
[d] Department of Eng. Mechanics and Theory of Structure, Faculty of Civil Engineering, University of Belgrade, Bulevar kralja Aleksandra 73, Belgrade 11000, Serbia
[e] EUCENTRE Foundation, Via Adolfo Ferrata, 1, Pavia, Italy

ARTICLE INFO

Keywords:
Multi-storey
Frame structure
Earthquake
Tank
Piping
Flange joints
Shaking table testing

ABSTRACT

Past earthquakes demonstrated the high vulnerability of industrial facilities equipped with complex process technologies leading to serious damage of process equipment and multiple and simultaneous release of hazardous substances. Nonetheless, current standards for seismic design of industrial facilities are considered inadequate to guarantee proper safety conditions against exceptional events entailing loss of containment and related consequences. On these premises, the SPIF project -Seismic Performance of Multi-Component Systems in Special Risk Industrial Facilities- was proposed within the framework of the European H2020 SERA funding scheme. In detail, the objective of the SPIF project is the investigation of the seismic behaviour of a representative industrial multi-storey frame structure equipped with complex process components by means of shaking table tests. Along this main vein and in a performance-based design perspective, the issues investigated in depth are the interaction between a primary moment resisting frame (MRF) steel structure and secondary process components that influence the performance of the whole system; and a proper check of floor spectra predictions. The evaluation of experimental data clearly shows a favourable performance of the MRF structure, some weaknesses of local details due to the interaction between floor crossbeams and process components and, finally, the overconservatism of current design standards w.r.t. floor spectra predictions.

1. Introduction

1.1. Background and Motivation

Most recent destructive earthquakes in China (Sichuan, 2008 and Yushu, 2010), Japan (Tohoku, 2011) and Italy (Emilia, 2012) highlighted the social and political consequences of seismic risk due to industrial facilities.

Several reports, like [1,2], along with a growing body of literature by European and United States researchers, e.g. [3,4], investigated numerous industrial accidents that have resulted in severe loss of life and injury, damage to natural and built environment, as well as significant economic losses. As past earthquakes have demonstrated, in critical facilities, interactions between supporting structures and plant components or process-related interactions are above all vulnerable and capable of leading more severe serious secondary damage. If hazardous substances are released due to loss of containement (LoC), in addition to loss of production, they also entail a major danger to both humans and environment. As many contributions demonstrated in literature, see, among others, in [5,6], seismic behaviour of support structures in major-hazard industrial/nuclear plants is therefore of paramount importance. Besides, recent studies [7,8] - [9], focused on the analysis and design of industrial and nuclear plant substructures equipped with process components such as pipes, tanks, etc. It is noteworthy that whilst several aspects in terms of design and analysis are still unresolved, code-compliant methods demonstrated to result in very poor predictions and often dated and inadequate, as highlighted in [10,11]. As a matter of fact, nowadays seismic provisions of industrial facilities are based on classical load-and-resistance factor design (LRFD), like EN 1998–1 [12], VCI-Guideline [13], or on allowable stress design (ASD), like ASME

* Corresponding author.
E-mail address: oreste.bursi@unitn.it (O.S. Bursi).

https://doi.org/10.1016/j.engstruct.2021.112681
Received 12 December 2020; Received in revised form 21 April 2021; Accepted 3 June 2021
Available online 17 June 2021
0141-0296/© 2021 Elsevier Ltd. All rights reserved.

B31.1 [14], ASME B31.3 [15] and EN 13480 [16], while a performance-based earthquake engineering (PBEE) approach should be preferred. In fact, the LRFD approach mainly guarantees an overall structural performance in terms of implicit targeted failure probability of individual structural components; conversely, the PBD methodology, through the law of total probability, can, naturally, link structural safety to seismic performance metrics, such as economic losses, downtime and above-mentioned fatalities. In this respect, criteria for design or retrofit solutions based on performance objectives are proposed and illustrated in [17]. While for civil-engineering structures- probabilities of exceedence of peak ground acceleration (PGA) *vs* limit states are clearly identified, little information can be found in literature for hazardous industrial equipment. Along this vein, a first attempt of correlation for petrochemical plants can be found in [18], where typical refinery piping systems were analysed referring to Operating Basis Earthquakes (OBEs) and Safe Shutdown Earthquakes (SSEs). The former corresponds to a probability of exceedance of 10% in 50 years and is defined as the condition under which plants remain fully functional without undue risk to health and safety of public. Increased return periods can be achieved through additional PGA multipliers. The latter is related to a lower probability of exceedance under which certain relevant structures, systems and important components must be designed to remain operational and allow a safe closure. For the sake of completeness, the OBE has been replaced by the design basis earthquake (DBE) in the last version of ASCE 4–16 [19]; from now on, we'll use this nomenclature. The importance of well-established relationships between limit states and reached damage in an industrial or nuclear system is clearly demonstrated by the consequences of failures of components in several accidents in industrial plants, as already illustrated in [1–4]. Consequences include the release of hazardous materials, human injuries and the increasing of overall damage to nearby areas, proving this to be a key emerging risk issue. More precisely, in view of quantitative seismic risk analysis (QRA) Caputo et al. [20] estimated consequences of some major-hazard process plants subjected to earthquakes. It emerged on one hand, a limited knowledge of the seismic behaviour of both critical units, components and support structures; on the other hand, the lack of information about their interactions. In fact, release of hazardous materials from secondary elements, i.e. pipes, tanks, etc., even not directly considered by current standards, could generate uncontrollable disasters, dramatically exacerbated by domino effects [21]. Therefore, researchers, [22,23], focused on the relation quantification between loss of containment (LoC) and seismic damage; moreover, since current design practice for piping systems contain little information about seismic component details [24], Bursi et al. [25] suggested innovative solutions based on non-standard bolted flange joints (BFJs). Along the same line, also the quantification of the behaviour factor q and the component response modification factor R_p, for European [26] and American [27] code respectively, for components on support structures has revealed to be inaccurate. For instance, while for piping systems [27] prescribes a R_p-factor in the range of $6-12$, [28] demonstrated through direct nonlinear analyses, values of R_p not greater than $3-4$. Besides, the authors explained this overestimation due to nonlinearities in the supporting structure which decreased the coupling effect and, hence, damage both in pipes and supports. Moreover, Bursi et al. [29] showed that a typical petrochemical piping system coupled with a steel support structure is endowed with a limited q factor, because both pipes and the support floors cannot ensure a rigid floor behaviour and a great involvement of dissipative elements. In addition, [30,31] demonstrated that the response of a piping system can be greatly reduced by including the nonlinear behaviour of local supports. Both the 2001 El Salvador [10] and the 2006 Hawaii earthquakes [32] have demonstrated that non-structural damage has clearly limited the functionality of critical facilities and, highlighted the importance of non-structural component performance. Furthermore, [33,34] underlined a definite lack of investigation as well as protocols for testing the interactions between primary structures and components under seismic loading. As regards the analysis of global systems based on PBEE, only a few studies can be found, see [33,29], among others, where interactions between structural elements and components have been performed. For instance, the application of PBEE to two realistic substructures of petrochemical piping systems showed a general overconservatism in piping system design. Conversely, some studies, e.g. the European research projects INDUSE 2009–2012 and INDUSE-2-SAFETY 2012–2015 [35] clearly focused on experimental testing of non-structural components and performance levels to be compliant with. More precisely, Bursi et al. [36] investigated the behaviour of non-standard BFJs endowed with plastic deformation capacity, and demonstrated that, in case of strong earthquakes, a limited localized plastification before LoC can be beneficial. To develop a better understanding of the elasto-plastic response and ultimate strength of nuclear power piping systems, other agencies carried out a multi-year test programme ([37]). As a result, in view of the enhancement of structural integrity of industrial, energy and nuclear components, design guidelines and recommendations were issued, [19–25,28–38].

Strictly related to PBEE, the development of involved nonlinear analysis methods for accurate evaluation of both limit states and damage represents another salient issue [39]. Step-by-step dynamic integration of a structural system, where explicit nonlinear behaviour of both primary and secondary components are considered, is clearly the most reliable analysis method. Nonetheless, simplified approach such as the use of nonlinear static analysis or the use of floor response spectra (FRS) are generally preferred. For instance, [40] demonstrated that common nonlinear static analyses cannot be used to assess the response of a coupled pipe-rack system. The main difficulty derives from the presence of non-building characteristics of this type of structures [27]. Both the absence of a rigid floor and the lack of dynamic interaction between primary (support) and secondary (components) system are among the main causes of discrepancies [41].Along the same vein, floor acceleration/displacement spectra represent a viable and promising approach which, however, has been applied to a lesser extent to the case of industrial and nuclear power plant structures; see, among others, [7–25,28–42]. For instance, Merino Vela et al. [7] focused on the development of floor acceleration spectra for an industrial concentrically braced frame supporting a liquid storage tank. The authors demonstrated that in most of the cases, code-compliant analytical approaches overpredict responses w.r.t. analyses that explicitly take into account the interaction between a supporting structure and a liquid storage tank. When [26] is used for the estimation of floor spectrum values, differences up to 30–35% were detected. Finally, Ezeberry and Combescure, [42], proposed a suitable methodology to determine seismic FRS at a particular location of a structural system by a direct method based on the frequency domain.

1.2. Scope

On these premises and to crystallize the ideas, both the interaction between primary and secondary elements that influence the performance of the whole system and proper and check of FRS predictions represent the main issues that the project SPIF want to investigate in depth in a PBEE perspective. Therefore, in order to fill the lack of experimental evidences, the SPIF project [43] has foreseen an experimental campaign of a representative industrial structure equipped with complex process technology subjected to shake table tests. Thus, the present paper, gathers the main characteristics of an archetype industrial facility, the test programme, and main results.

In particular, Section 2 describes the case study, a steel 3-levels prototype of an industrial plant structure equipped with typical industrial components such as vertical and horizontal tanks, cabinet and pipes with elbows, special flanges and T-joints; also the sensor layout is presented. Then, Section 3 deals with the definition of the test programme and the seismic input selection. More precisely, shaking table tests, characterised by spectrum-compatible accelerogram levels ranging from

0.16*g* to 0.71*g* PGA, have been performed. In Section 4, a significant amount of acquired data is assessed and system identification of modal frequencies, mode shapes and damping coefficients through a rational fraction polynomial (RFP) method are carried out. The definition of relationships between damage levels, limit states and performance of components are carried out in Section 5. Moreover, comparisons between FRS estimated through experimental data and those evaluated in compliance with codes and standards are also performed, resulting the latter in a clear underestimation when close to the resonance condition. Finally, conclusions and future developments are drawn in Section 6.

2. Experimental Mock-up and Setup

2.1. Mock-up Description

The full scale mock-up consists of a primary steel structure supporting horizontal and vertical tanks, piping installations and a cabinet. Furthermore, a conveyor was placed on the reinforced concrete slab without any connection to the main structure. It was conceived as a three-storey steel frame with flexible diaphragms made of crossbeams hinged to the frame beams. Fig. 1 shows the test structure on the shaking table with different views on each storey; Fig. 2a, instead, depicts the top view of the CAD model. The dimensions of the structure are 3.7 m x 3.7 m in plan with a storey height of 3.1 m, which leads to a total height of 9.3 m. The columns were fully clamped to a reinforced concrete base plate. This latter has dimensions of 4.8 m x 4.8 m and a thickness of 0.4 m and was constructed with a concrete of class C30/37. The horizontal load bearing system of the steel structure consisted of two moment resisting frames (MRFs) in the direction of the seismic excitation and two braced frames in the transverse direction equipped with tension/compression bracings with circular cross section. These latter were used in order to limit lateral movements and torsional effects. The arrangement of the profiles on each storey level is shown for the first storey in Fig. 2b. The two MRFs were connected through crossbeams, which are fastened to the frame beams by simple bolted connections with web stiffeners as shown in Fig. 2c. These crossbeams served in turn as bearing supports for bearing platforms which were installed with bolted connections to place the secondary elements. In particular, HEA220 profiles were used for columns, whereas HEA200 and HEA180 profiles were employed for the longitudinal girders on the first level and the remaining ones, respectively.

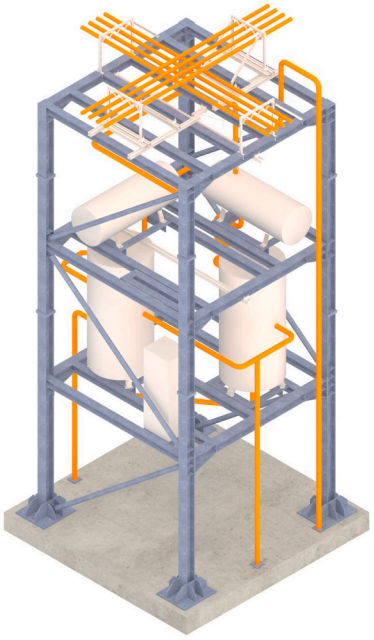
Moreover, the transversal beams were made of HEA160 profiles, the horizontal frames with L-Profiles (160 x 160 x 15 mm) and the diagonal bracings with a tube of cross Section 101.6 x 3 mm. All profiles were made of steel grade S355. The MRF joints were bolted connections with welded stiffeners and haunches; whereas, diagonal bracings were connected to the columns using bolted connections as well. The bearing platforms were bolted to the crossbeams. All bolted connections were realized with bolts M16 with grade 10.9. The columns of the steel frame were welded on steel anchor plate of 30 mm thickness which, in turn, were anchored to the reinforced concrete slab. The anchorage system was composed of a combination of both special chemical anchors and continuous anchors. More precisely, five M30 anchors per column, going all the way through the concrete slab, were used, along with three M24 bars chemically anchored to the slab. In addition, to guarantee the necessary stiffness and strength of column base joints, they were equipped with six stiffeners of 20 mm thickness, welded both to the column and to the anchor plate as depicted in Fig. 3.

The secondary elements of the industrial structure included tanks, pipes, elbows, bolted flange joints (BFJs), tee-pipe joints (Fig. 6 and a cabinet, see Fig. 4.

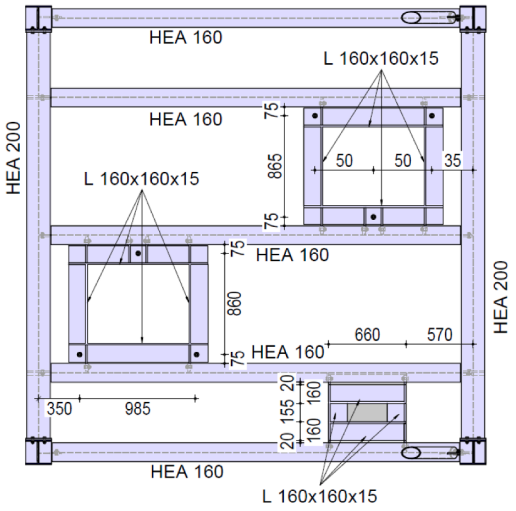
Four unpressurized tanks made of steel S235JRG2 with a yield strength of 235 N/mm^2 were installed: two vertical tanks on the first floor, i.e. Tank #1 and #2; and two horizontal tanks on the second floor, i.e. Tank #3 and #4, respectively. Their locations are shown in Fig. 8. In order to simulate the liquid typically stored in such tanks, they were filled with granular material with a density equal to water. This allowed for the protection of the shaking table and the technical installations against liquid release. The geometry and dimensions of the tanks are shown in Fig. 5. In particular, both vertical tanks were 2.76 m high, with a diameter of 1.25 m and a thickness of 5.6 mm, with a self-weight of around 0.65 tons. They were supported on three symmetrically positioned supports, 120° apart from each other. They were endowed with a filling capacity of 3000 liters and were filled up to 80 percent of their capacity, which resulted in an additional mass due to filling of 2.4 tons. Each support of the tank was fastened to the corresponding bearing platform with a M20 bolt of grade 10.9. The horizontal tanks were instead 2.12 m long, with a diameter of 0.8 m, a thickness of roughly 3.9 mm and a self-weight of about 0.3 ton. They were supported on four symmetrically positioned supports, 1.14 m apart from each other in length. They are endowed with a filling capacity of 1000 liters and were filled up to 80 per cent of their capacity, which resulted in an additional



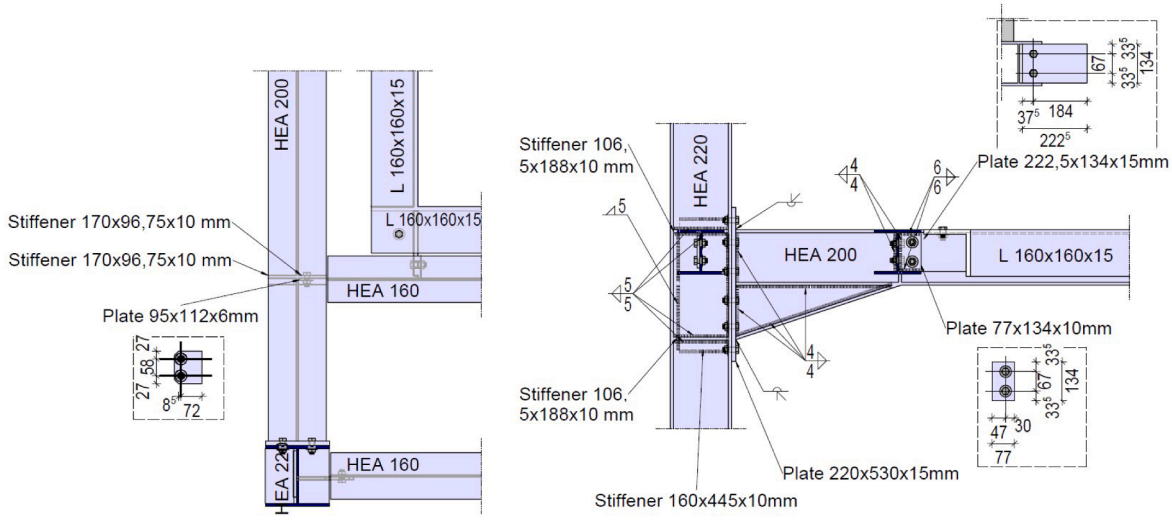
Fig. 1. Mock-up photographs at the EUCENTRE Laboratory.



(a) CAD-Model



(b) Top view: First storey



(c) Connections of crossbeams (HEA 160) to the MRF and bearing platforms (L 160x160x3)

Fig. 2. Primary steel structure.

mass due to filling of 0.8 ton.

The tanks were mutually connected to each other through a piping system consisting of nine DN100 pipes, with a 100 mm diameter and a 3.6 mm thickness. Some pipes were also connected to the concrete slab. The relevant pipe layout is shown in Fig. 6a, and consists of straight branches, elbows and tee pipe joints. The material used for the pipes was P235 with a yield strength of $235 N/mm^2$. Moreover, a suspended pipe rack was also installed on the third floor which is endowed with DN80 pipes. The pipe positions #1, #3 and #5, see Fig. 6, were attached to the concrete slab through a 20 mm thick baseplate, which was welded to the pipes and bolted to the concrete plate with 4 x M16 injected bolts at each plate. Moreover, bolted flange joints were necessary in order to connect the several parts of pipe. More precisely, the loose flanges adjacent to the tanks were conceived as moving flanges, while the others were simple flanges welded to pipes. Both flange joints can be observed in Fig. 6. Moreover, the pipe branches with the most critical bolted flange joints, i.e.Pos #1, Pos #4, Pos #5 and Pos #6 were filled with water and pressurized at 20 bars. The filling was conducted after the pipes had been installed, through retaining valves integrated into the pipes. The fastening and positioning of the pipes were accomplished by implementing a channel support system. This consisted of a series of girders with a hollow square cross section of 90 mm x 90 mm in different lengths that were clamped to the steel structure.

The pipes were held in place either by a U-bolt, that prevented them from a horizontal movement, or by a beam clamp, i.e. Pos #4 and Pos #9, that prevented them from a vertical movement. Additionally, the support of Pos #9 was accompanied by a truss system, made of steel rods, that also held the pipes horizontally in place.

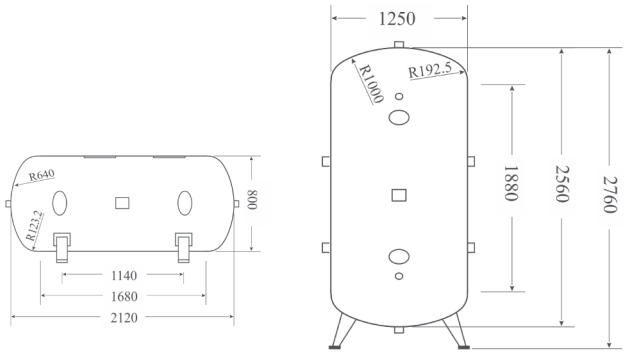
The different configurations are again illustrated in Fig. 6. In total eight pipes, each 4.9 m long, were installed: four parallel to the motion direction and four in the orthogonal direction as shown in Fig. 7. The pipes were secured to the main structure with frames and were suspended with beam clamps connected through a steel rod as depicted in Fig. 7. The pipes were also sealed at both ends, as they were completely filled with water. Finally, an electrical cabinet was installed on the first level of the primary structure with dimensions H x L x B = 1.82 x 0.56 x



Fig. 3. Typical anchorage of columns to the reinforced concrete plate: base plate with welded stiffeners and anchors.



Fig. 4. Cabinet on the first floor.



(a) Vertical tank (b) Horizontal tank

Fig. 5. Geometry of the vertical (a) and horizontal (b) tanks.

0.66 m and a weight of about 140 kg. The cabinet was secured to the platform with four M12 bolts of strength class 10.9.

2.2. Sensors Layout

A series of sensors was positioned on both the primary structure and secondary units. The instrumentation consists of accelerometers, displacement transducers (LVDTs) and strain gauges (SGs). The distribution of the sensors is summarized in Table 1. In particular, in order to analyze the dynamic behaviour of both the primary structure and secondary units a total of 54 uniaxial accelerometers have been placed at various floors and on the tanks. The location of the accelerometers is summarized in Fig. 8. In particular, in order to identify the seismic input to which the structure was actually subjected to, three accelerometers A #2, A #3 and A #4 were installed on the RC slab. Moreover, data provided by the accelerometers at each floor allowed for the dynamic identification of the primary structure and the definition of floor response spectra. Accelerometers A #9, A #12, A #17 and A #18, located respectively on Tank #1, Tank #2, Tank #3 and Tank #4, allowed for the dynamic identification of the equipment; while two accelerometers A #8 and A #11 placed at the base of the vertical tanks were used to quantify floor accelerations. In order to evaluate the local behaviour of the primary steel structure, a series of LVDT transducers and SG sensors were installed as indicated in Fig. 8. More precisely, in order to monitor uplift of base joints LVDT #3 to LVDT #10 were installed in the vertical direction between the column base plate and the RC slab; conversely, to estimate the average curvature and the axial deformation of member cross sections, strain gauges were installed at the base of columns.

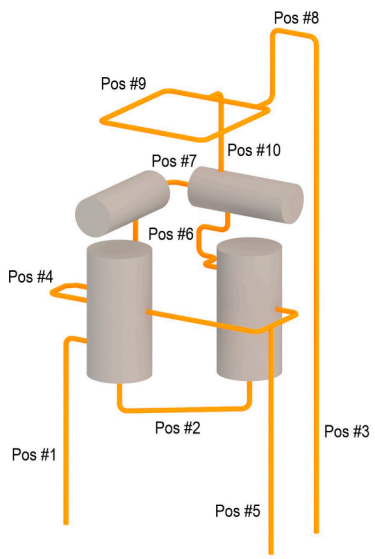
The most critical BFJs of the piping system, i.e. Pos #1, Pos #4, Pos #5 and Pos #6 shown in Fig. 9, were monitored by using LVDTs and SGs. In particular, with the aim to quantify strain amounts during seismic excitations and check possible yielding three SGs were installed on pipes just close to flange joints. Furthermore, in order to monitor the flange opening and to derive the relative rotation of flanges during seismic loading, three LVDTs were installed in each BFJ with an angular distance of 120°. In addition, with the aim to monitor a potential drop of pressure due to leakage, a pressure transducer was installed in each flange.

The displacement sensor setup was also complemented with an optical measurement system, made of 78 markers applied to different points of both the primary structure and secondary elements. They are indicated in Fig. 10. In order to allow for estimation of both local and global movements they were tracked by 16 cameras equipped with infrared sensors for movement recording.

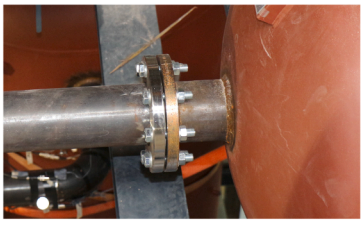
3. Selection of seismic input and Test Programme

3.1. Performance Based Design and Reference Limit States

In order to define proper limit states for the multi-storey frame with process equipment, we recall the main goals of the SPIF project i.e. the quantification of the interaction between the primary MRF structure and process components and a proper check of floor spectra predicted by standards and specialised literature. With respect to the first objective and according to the PBEE approach [44,45], the primary structure was designed to cope with the *Near Collapse* (NC) limit state; as a result, a severe earthquake prone-scenario was assumed leading to a design PGA of 0.69 g. Conversely, the secondary process components were designed according to nowadays common pratice; nonetheless, these components satisfy both the DSE and SSE requirements [46]. Therefore, in agreement with the cited standards, for the primary structure we correlated different limit states to PGA levels as collected in Table 2; whilst Table 3 gathers limit states to PGA levels for process plant components. Those PGA values were considered in the test programme discussed in Sub-Section 3.3. In view of the preliminary design of the test structure, two



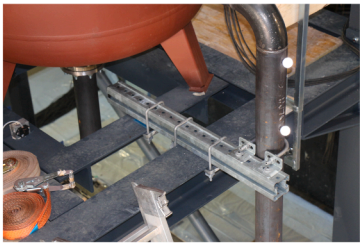
(a) Secondary elements layout



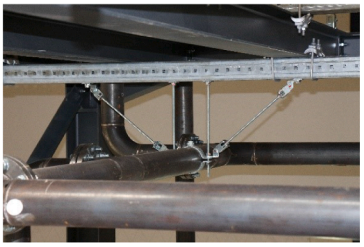
(b) Loose flange joint pipe Pos #2



(c) Base plate pipe Pos #3



(d) Girder with U-bolt pipe Pos #1



(e) Girder with rod bracing Pos #9

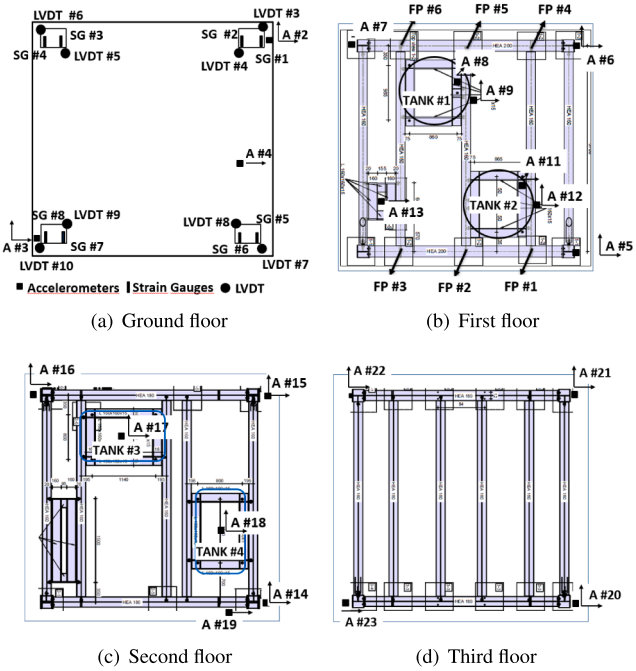
Fig. 6. Piping system and layout.



Fig. 7. Pipe rack on the third floor.

Table 1
Sensors type and numbers in the mock-up.

Level	Accelerometer	LVDT	Strain gauges
Floor 0	6	15	12
Floor 1	16	-	-
Floor 2	11	-	-
Floor 3	7	-	-
Roof top	14	4	-
Pipes (Pos. 1, 4, 5, 6)	-	12	12



(a) Ground floor (b) First floor

(c) Second floor (d) Third floor

Fig. 8. Sensors location at each floor.

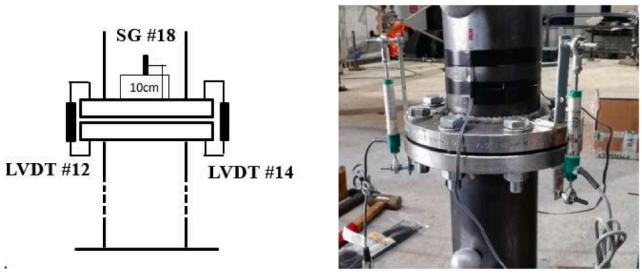
models of different complexity were used: i) a simplified model with secondary components idealized with concentrated masses and subjected to elastic and pushover analysis; ii) a sophisticated model, characterised by a detailed discretization of secondary components and connecting pipes and devoted to damage analyses, subjected to nonlinear time histories.

3.2. Spectrum-compatible Accelerograms

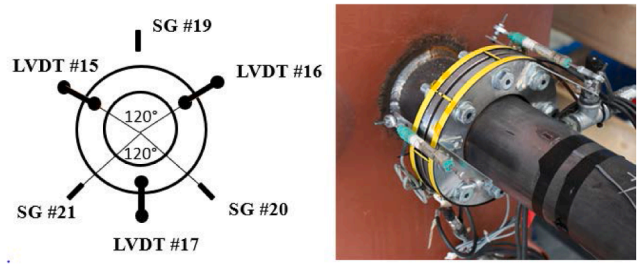
The applied seismic action was based on a linear elastic response spectrum Type 1, with soil condition C, a PGA = 0.6 g and a damping ratio of 5 %, in agreement with Eurocode 8-Part 1 [12]. The spectrum, depicted in Fig. 11, exhibits a spectral acceleration, $S_a(T = 0) = 0.63$ g and a plateau between 0.2 s and 0.6 s with a maximum value $S_a(T = 0.2 \div 0.6) = 1.725$g.

In compliance with the aforementioned spectrum, a set of 10 stochastically independent accelerograms, TH #1-TH #10, was generated.

The simulations conducted on a finite element (FE) model of the mock-up, with all generated accelerograms, allowed for the identification of the accelerogram TH #8, due to the relative amount of damage induced. In this respect, Fig. 12 shows the acceleration time history TH #8 for a reference PGA of 0.63 g and its corresponding velocity and displacement time histories. The signal was applied through the shaking table with a sampling rate of 256 Hz, a total duration of 25 s and a baseline correction. The spectrum tolerance, i.e. the accepted difference between the spectrum of each generated accelerogram and that of the



(a) BFJ Pos #4 - Top and side view



(b) BFJ Pos #1 - Top and side view

Fig. 9. Piping monitoring: sensors location on the BFJs.

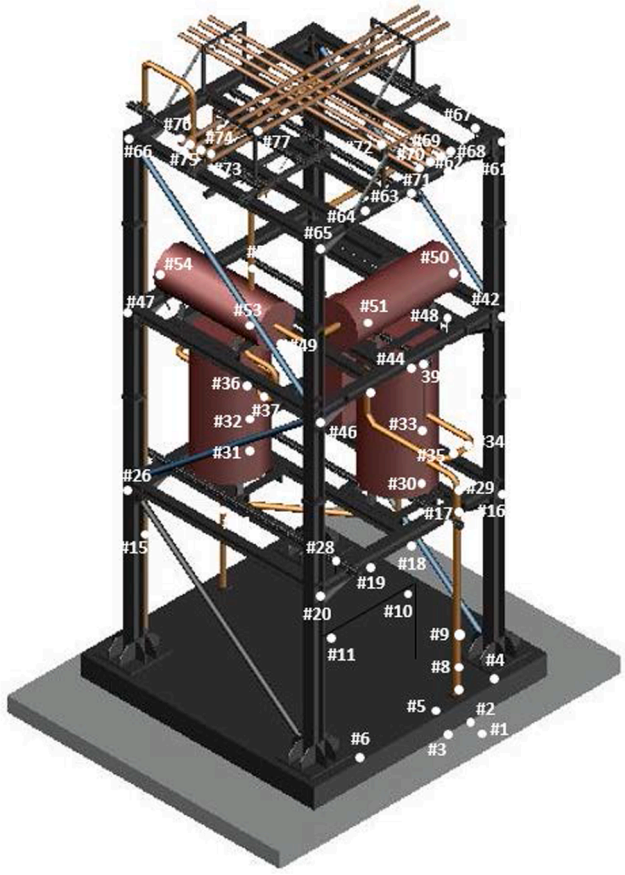


Fig. 10. Markers layout.

target spectrum, was satisfied with an absolute value of 0.1. The generation of accelerograms was based on a quadratic baseline correction. Moreover, during signal generation, the compatibility with the shaking table was checked both in terms of velocity and displacement capacities; therefore, no further signal filtering and processing was needed.

Table 2
Significant limit states for primary structures.

Limit States			P_{V_R}		T_R	S.F.	PGA
Fully Operational	-	**OP**	81	%	75	0.31	0.22
Damage Limitation	-	**DL**	63	%	125	0.37	0.26
Significant Damage	-	**SD**	10	%	1188	0.79	0.54
Near Collapse	-	**NC**	5	%	2438	1.7	0.69

Table 3
Significant limit states for process plants.

Limit States		P_{V_R}			T_R	S.F.	PGA
Operating Basis	-	**DSE**	10	%	1200	0.80	0.54
Safe Shutdown	-	**SSE**	5	%	2475	1.01	0.69

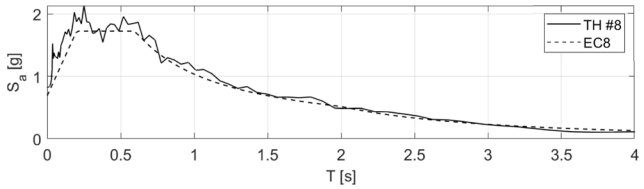
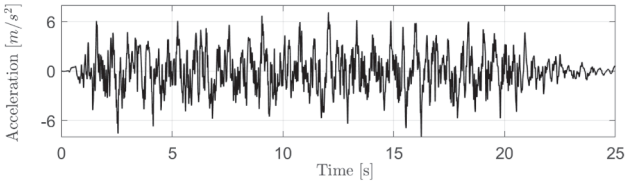
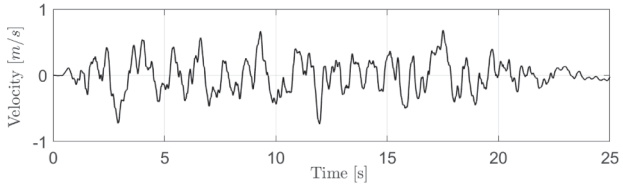


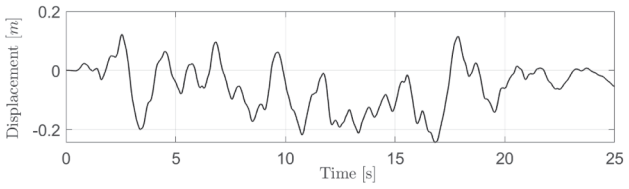
Fig. 11. Eurocode 8-Part 1 Target spectrum and artificially generated spectrum for time histories TH #8.



(a) Acceleration time history



(b) Velocity time history



(c) Displacement time history

Fig. 12. Artificially-generated time histories TH #8.

3.3. Test Programme

The objective of the test programme was to impose different PGA levels -defined in Tables 2 and 3- to the test structure. Besides, in view of the tuning of the shaking table and the dynamic identification of the mock-up, a series of tests with random excitation and low PGA levels ranging between 0.05 g and 0.15 g were performed. Thus, the seismic excitation was then scaled with respect to (w.r.t.) the design PGA of 0.63 g to 25 %, 37 %, 50 %, 70 %, 100 % and 110 %. For the sake of

clarity, white noise random excitation signals with constant power spectral density (PSD) in a certain frequency range, are commonly used in the progressive system identification of mock-ups tested on a shake table. Therefore, the reference for the random excitation was a constant root mean square (RMS) intensity on frequencies in the range of 0.5–50 Hz, with the aforementioned PGA levels. A higher intensity allows for a better signal tracking and a higher signal-to-noise ratio; nonetheless, excessively high intensities may produce unwanted inelastic responses.

The testing campaign and the corresponding nomenclature is collected in Table 4. In detail, the first two runs were conducted with the random excitations RND #13 and RND #15. Successively, runs with PGA levels of 0.16 g, 0.23 g and 0.31 g were carried out. Before the test to be conducted at a level of 0.44 g, a further tuning of the shaking table was performed with a random excitation RND #16 and a relevant seismic excitation at 0.23 g PGA.

After the successful completion of the test with a PGA level of 0.44 g, a last tuning phase was performed with a random excitation RND #17 and a seismic excitation with 0.23 g PGA. The final tests were executed for the maximum levels of 0.64 g and 0.71 g PGA. Lastly, a closing test with the random excitation RND #18 was carried out.

4. System Identification and Observations

In this section, the dynamic identification of the SPIF structure and relevant observations on the experimental campaign are discussed.

4.1. Identification of frequencies, mode shapes and damping ratios

The transition from raw data into systems' performance meaningful information, see SubSection 4.2, requires the adoption of proper system identification (SI) methods [47]. Within the framework of SPIF, two approaches have been followed: i) the adoption of the PSD of recorded accelerometers' signals, to estimate accurate frequencies' shifts and rapid checks on the structural behaviour of the mock-up along the experimental campaign; ii) the use of rational fraction polynomials (RFP) applied to frequency response functions (FRFs) in order to achieve a more reliable estimate of frequencies, mode shapes and, especially, damping ratios.

In order to reduce interference from unwanted noise due to power lines or power supply ripple, a finite impulse response (FIR) low-pass filter with cutoff frequency of 30 Hz was applied to recorded signals. In particular, the FIR filter uses a least-squares approximation to compute the filter coefficients and then smooths the impulse response with a Hamming window. Then, for each acquired time-history of accelerometers both fast Fourier Transform (FFT) and power spectrum density (PSD) based on the Welch's method have been performed. In particular, the discrete PSD P_{yy} reads,

$$P_{yy}[i] = \begin{cases} \dfrac{Y[i]\cdot Y[i]^*}{NG\cdot F_s/N}, & \text{if } i = 0 \\ \dfrac{2\cdot Y[i]\cdot Y[i]^*}{NG\cdot F_s/N}, & \text{otherwise} \end{cases} \quad (1)$$

where, to obtain a clear spectral representation of the time series $x[i]$, the Hamming window $w[i]$ has been used as follows,

$$Y[i] = \frac{1}{N}\mathrm{FFT}\{x[i]\cdot w[i]\} \quad (2)$$

In Eq. 1 * stands for transpose, $Y[i]$ has been firstly normalized by the noise gain, $NG = \frac{1}{N}\sum_{i=0}^{N-1} w[i]^2$ and, finally, divided by the sampling frequency, F_s, over the total length N of the signal.

Results of SI either along the MRF direction, i.e. the shaking direction, and the orthogonal BF direction are reported in Fig. 13, for both Random #13 and Random #18, listed in Table 4.

The response of the structure along the MRF direction, subjected to random inputs of PGA intensity in the range $0.05g - 0.15g$, allows to reliably estimate the first frequency around $2.9\,Hz$ and other frequencies at $6.0\,Hz$, $9.0\,Hz$ as other main frequencies. There is also a peak around $5.0\,Hz$, especially pronounced with FFT's signals recorded at the 3^{rd} floor.

Instead, for the same random excitation along the BF direction, peaks near $5.2\,Hz$ and $7.2\,Hz$ have been identified. Obviously, they exhibited a minor amplitude in comparison with the MRF direction; this can be observed from the PSD amplitudes of Fig. 13.

The resulting identified frequencies for all random signals are collected in Table 5. A careful reader can notice that till 70% of TH #8 the overall system exhibits a linear response; therefore, the identified frequencies gathered in Table 5 remain almost unchanged. Nonetheless, it is worth noticing that Random #18 is the only random signal adopted after TH #8 at 110% and, therefore, some damage happened in the fin plate connection D-FP #1 between a primary and a secondary beam depicted in Fig. 8. As a result, a reduction in frequency is evident in Table 6 in terms of percentage.

As mentioned above, data have also been processed by means of the RFP, [48]. This technique overcomes many of the numerical analysis

Table 4
Nomenclature, characteristics and synthetic observations of SPIF Test Programme.

Label	Excitation	State	Scaling factor	PGA Level	Observations
RND #13	Random	DSE - OP	-	0.05 g - 0.15 g	- Overall elastic linear behaviour
RND #15	Random	DSE - OP	-	0.05 g - 0.15 g	- Overall elastic linear behaviour
TH #8–25%	Seismic	DSE - OP	25%	0.16 g	- Overall elastic linear behaviour
TH #8–37%	Seismic	DSE - OP	37%	0.23 g	- Overall elastic linear behaviour
TH #8–50%	Seismic	DSE - DL	50%	0.31 g	- Overall elastic linear behaviour
RND #16	Random	DSE - OP	-	0.05 g - 0.15 g	- Overall elastic linear behaviour
TH #8–37%	Seismic	DSE - OP	37%	0.23 g	- 3^{rd} floor: collapse of pipe rack in the transversal direction
TH #8–70%	Seismic	DSE - DL	70%	0.44 g	- Large displ. ($\pm 30\,mm$) of vertical Tank #2 at the 1^{st} floor - Relevant rotation of the cross beam under the vertical Tank #2 and warping of the web of fin plate D-FP #1 - Strengthening of the cross-beam underneath Tank #2 in correspondance of D-FP #1
RND #17	Random	DSE - OP	-	0.05 g - 0.15 g	- Overall elastic linear behaviour
TH #8–37%	Seismic	DSE - OP	37%	0.23 g	- Overall elastic linear behaviour
TH #8–100%	Seismic	SSE - SD	100%	0.64 g	- D-FP #2,5,6 fin plate experienced cracking
TH #8–110%	Seismic	SSE - NC	110%	0.71 g	- Cracking on previously detail D-FP #2,5,6 significantly increased - Failure of bracing supporting the conveyor
RND #18	Random	DSE - OP	-	0.05 g - 0.15 g	- Overall elastic linear behaviour

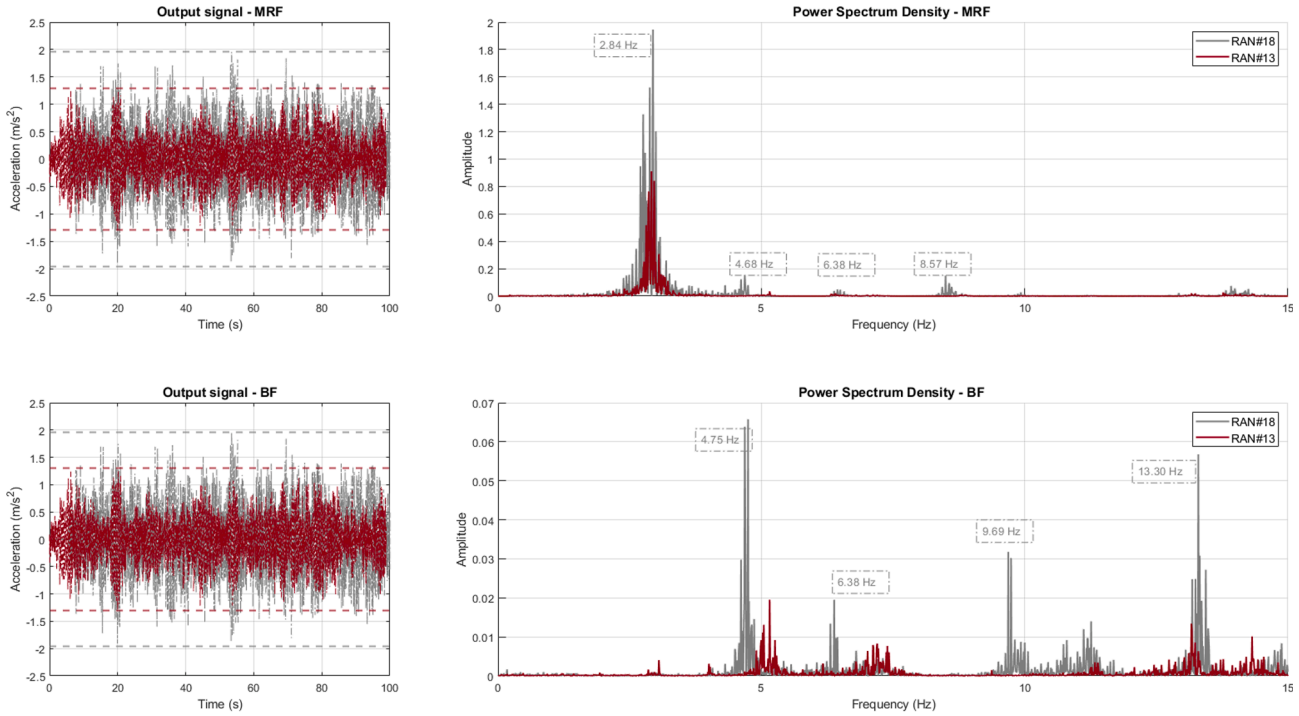


Fig. 13. Acquired signal and PSDs either on MRF and BF direction for Random #13 - excitation at the beginning of the test programme - and Random #18 - excitation at the end of the test campaign -, respectively: a shift to the left of frequencies especially those in the BF direction is evident..

Table 5
Identified frequencies from Random signals through PSDs analyses along the MRF direction. Also Δ[%] variations between current and initial frequencies are reported.

	MRF Direction							
	$f_{n1}[Hz]$	Δ[%]	$f_{n2}[Hz]$	Δ[%]	$f_{n3}[Hz]$	Δ[%]	$f_{n4}[Hz]$	Δ[%]
Random #13	2.91	-	5.20	-	6.33	-	8.73	-
Random #15	2.87	−1.37	5.17	−0.58	6.41	1.26	8.87	1.60
Random #16	2.88	−1.03	5.13	−1.35	6.36	0.47	8.82	1.03
Random #17	2.86	−0.35	4.99	−3.48	6.33	−1.25	8.62	−2.82
Random #18	2.84	−2.41	4.68	−10.00	6.38	0.79	8.57	−1.83

Table 6
Identified frequencies from Random signals through PSDs analyses along the BF direction. Also Δ[%] variations between current and initial frequencies are reported.

	BF Direction							
	$f_{n1}[Hz]$	Δ[%]	$f_{n2}[Hz]$	Δ[%]	$f_{n3}[Hz]$	Δ[%]	$f_{n4}[Hz]$	Δ[%]
Random #13	5.21	-	7.12	-	-	-	14.48	-
Random #15	5.01	−3.84	7.10	−0.28	-	-	14.45	−0.21
Random #16	4.94	−5.18	7.13	0.14	-	-	14.38	−0.69
Random #17	4.95	−1.20	7.14	0.56	10.12	-	13.52	−6.44
Random #18	4.75	−8.83	6.38	−10.39	9.69	−4.25	13.30	−8.15

problems associated to parameter estimation of structures, such as damping ratio estimation, high computational burden for processing, etc.; moreover, it allows for a precise identification of poles, zeros and resonances. Firstly, we compute the matrix of frequency response functions (FRFs) obtained from excitation signals of the shaking table and the corresponding response signals of the whole structure, processed at a sampling rate of 256 *Hz*. Then, in order to define system's transfer function we perform the ratios between input and outputs in the frequency domain. Therefore, we assume that the response to the input applied at location q is measured at location p, and thus, the related FRF can be expressed as follows,

$$H_{pq}(\omega) = \frac{Y_p(\omega)}{F_q(\omega)} = \frac{\sum_{k=0}^{n} \beta_k (i\omega)^k}{\sum_{h=0}^{m} \alpha_h (i\omega)^k} \tag{3}$$

For a generic single input-multiple output (SIMO) case, Eqn. 3 can be expressed in matrix form in the unknown α_h and β_k terms as,

$$\sum_{h=0}^{m} \left(\left[\alpha_h\right](i\omega)^k \right) \cdot \left[H(\omega)\right] = \sum_{k=0}^{n} \left(\left[\beta_k\right](i\omega)^k \right) \tag{4}$$

Therefore, by curve fitting the aforementioned analytical form to measurement data, the unknown coefficients ($\alpha_h, h = 0, \ldots, m$) and ($\beta_k, k = 0, \ldots, n$) of both the numerator and denominator polynomials can be

determined in a least-squared-error sense, [48].

Successively, it was possible to evaluate damped frequencies and mode shapes. As demonstred by several authors [49,50]-[51], indeed, the denominator of the RFP holds the information about the poles or eigenvalues of the structure, whilst the numerator holds the information about the mode shapes or eigenvectors of the dynamic system.

More precisely, the poles $\lambda_r = \sigma_r + i\omega_{d,r}$, that hold the information about damped frequencies $f_{d,r} = \omega_{d,r}/2\pi$, are obtained as roots of the denominator polynomial; the mode shapes instead are provided by the numerator. Moreover, damping ratios are calculated as $\xi_r = -Re(\lambda_r)/|\lambda_r|$, where r denotes the relevant mode shape number. For the sake of brevity, Table 7 summarizes the main results in terms of eigenvalues -frequencies - whilst damping ratios and some mode shapes are reported in Fig. 14. A careful reader can observe a slight decrease of frequency values in the DSE range, i.e. from 2.88 Hz to 2.86 Hz for f_{n1}; a frequency jump from the DSE to the SSE range, i.e. from 2.86 Hz to 2.76 Hz always for f_{n1}. Moreover, the high stiffness values of the BF system w.r.t. the MRF system is evident in the f_{n1} values.

To be thorough, the coherence function $C_{xy}(\omega)$ has been evaluated as

$$C_{xy}(\omega) = \frac{|P_{xy}(\omega)|^2}{P_{xx}(\omega)\cdot P_{yy}(\omega)} \tag{5}$$

where P_{xx} and P_{yy} denote power spectral densities of the input, x and output y signals, while P_{xy} denotes the cross power spectral density of x and y. In particular, the coherence represents a useful tool to discriminate whether detected peaks correspond to real frequencies or to artefacts of disturbances. As it can be observed in Fig. 15, the coherence function is close to unity for frequency values collected in Tables 5 and 7, while tends to zero for artefact or mismatched frequencies. Moreover, based on magnitude and phase of FRFs, mode shapes of the tested structure have been derived and reported in Fig. 14. In particular, mode shapes are illustrated for frequencies $f_n = 2.88 - 4.24 - 6.38 - 9.17\,Hz$. In addition to expected mode shapes for MRF and BF structures, a certain coupling of the aforementioned systems can be noticed at $f_n = 8.95\,Hz$. Finally, based on gathered data from Tables 5–7, it may be argued that the PSD approach allows for a reliable detection of frequency variations and a rapid check of system's performance during experimental phases. Conversely, the RFP method exhibits a better performance w.r.t. PSD; in fact, it allows for frequency shift detection, a more accurate peak amplitude evaluation and, especially, mode shape and damping estimations.

4.2. System performance

Main observations and comments on the structural response of both primary systems and process units subjected to the test programme listed in Table 4 are summarized herein. From Table 4, the main structure and the process components behaved elastically. The elastic regime is confirmed by sensors and visual inspection of the mock-up that resulted in no damage detection both in the primary structure and secondary elements.

4.2.1. Main structure response and damage

The seismic response of the MRF frame can be appreciated in terms of both floor accelerations and displacements for each run of the test programme; for the sake of brevity, only time histories relevant to the record TH #8–110% are depicted in Fig. 16. From Fig. 16a a careful reader can observe the high values of accelerations experienced by the MRF frame; moreover, no-residual displacements in sensors' data were recorded, see Fig. 16b, in agreement with the aforementioned observed elastic regime of the MRF frame. Also strain values at base columns, highlighted in Fig. 17 and located as depicted in Fig. 8, confirm the elastic behaviour of the main structure up to TH #8–110%; both SGs #1 and #8 associated to the most stressed column, showed indeed strain levels quite far from the yielding condition, characterized by a strain value of 1.7‰.

In addition, by the data acquired from markers located in Fig. 10, the motion of the whole structural system was reconstructed. With regard to the main structure, it is worthy to show in Fig. 22, the diaphgram floor displacement for each of the three storeys due to the last seismic run TH #8–110%. One can observe that the MRF frame experiences a limited torsional behaviour and each floor practically keeps its original shape. Although the overall behaviour of the primary steel structure appears rather linear from the data recorded by the sensors, during the test with TH #8–70% large displacements of Tank #2 of about 25 mm caused additional rocking on the supporting crossbeams. As a consequence, the interaction between the main beams of the MRF frame and the crossbeams caused damage to the fin plate joint FP #1. The location of the FP #1 on the first floor is reported in Fig. 8 and building details are shown in Fig. 2c. More precisely, the FP #1 fin plate connection experienced warping of crossbeam's web and cracks in the transition zone from beam to web. After the run TH #8–70%, in order to avoid collapse due to the strong interaction at higher PGA levels, the crossbeam underneath Tank #2 was strengthened by a bolted tee stub as depicted in Fig. 18. The crack initiation, propagation and the entailing warping was then more consistent in the subsequent runs with higher PGA-levels also on other crossbeams, i.e. fin plate FP #3, FP #4 and FP #6 labelled in Fig. 8. The last test carried out with the record TH #8–110% entailed additional damage on fin plate connections, especially in connections FP #2 and FP #5, see Fig. 19c, underneath both vertical tanks.

4.2.2. Secondary components system response and damage

Secondary elements seismic response has been analyzed in terms of both accelerations and displacements for each run of the test programme. As anticipated, both vertical and horizontal tanks were monitored. In particular, we focused our attention on vertical Tank #2 -with sensor A #12- and horizontal Tank #4 - with sensor A #18-. In this respect, both absolute acceleration and relative displacement at the top of Tank #2 -between markers #36 and #5- and Tank #4 -between markers #53 and #42- subjected to the record TH #8–110% are shown in Fig. 23a. One can observe that accelerations on the vertical tank are similar to the ones of the horizontal tank, even though the horizontal tank is located on a second floor that has higher floor accelerations than the first level. Fig. 23b depicts the relative displacement of Tanks #2 and

Table 7
Identified frequencies by the RFP's signal analysis on the TH #8 excitation both for the MRF and BF directions. The horizontal line separates OBE from SSE seismic inputs.

	MRF Direction			BF Direction		
	f_{n1} [Hz]	f_{n2} [Hz]	f_{n3} [Hz]	f_{n1} [Hz]	f_{n2} [Hz]	f_{n3} [Hz]
TH #8–25%	2.88	6.42	9.17	4.24	6.38	9.33
TH #8–37%	2.88	6.38	9.19	4.11	6.30	9.21
TH #8–50%	2.86	6.38	9.06	4.07	6.30	9.17
TH #8–37%	2.86	6.36	8.94	4.06	6.22	9.15
TH #8–70%	2.85	6.35	8.83	4.03	6.32	9.12
TH #8–37%	2.86	6.55	8.84	4.05	6.29	9.15
TH #8–100%	2.76	6.39	8.87	4.01	6.26	9.16
TH #8–110%	2.75	6.20	8.90	4.01	6.27	9.13

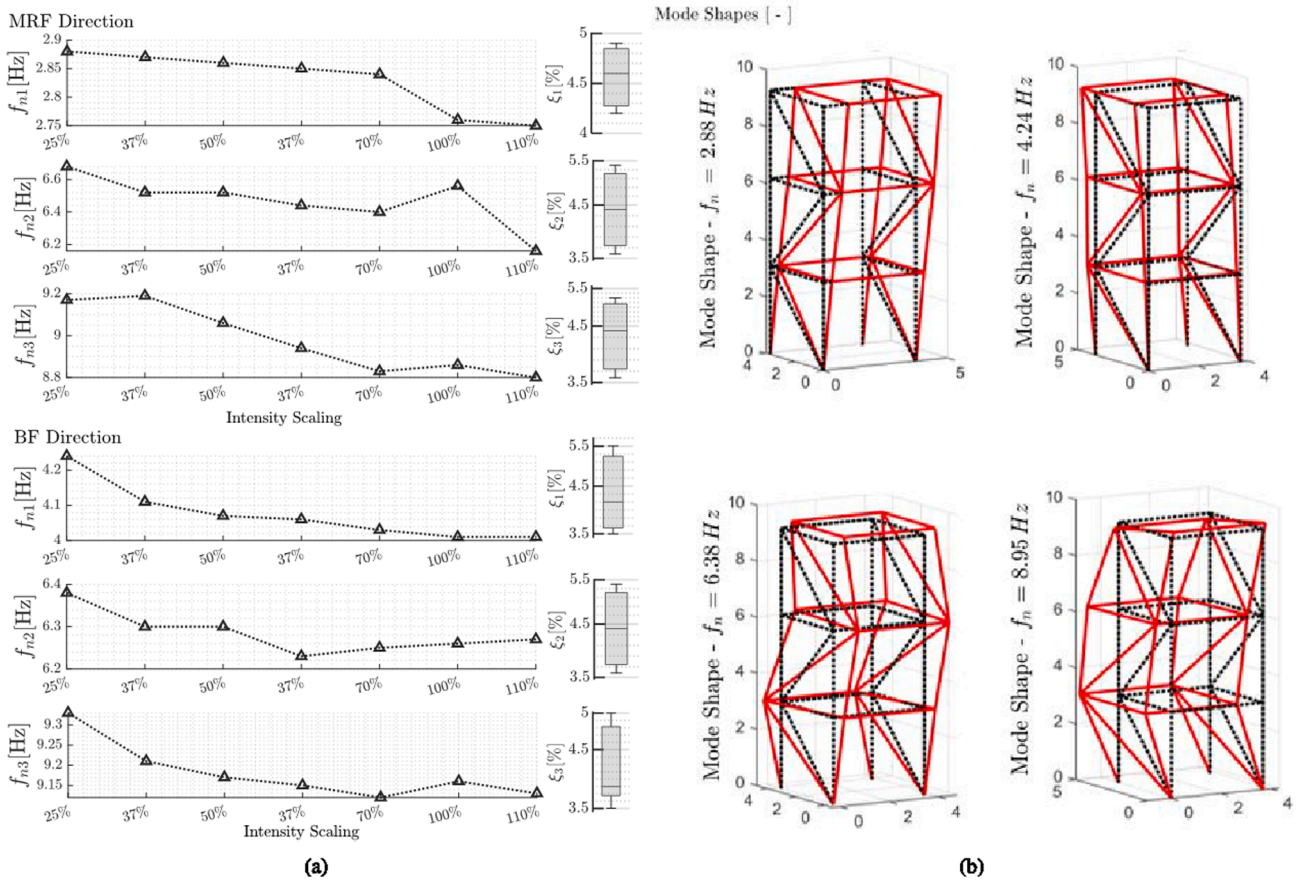


Fig. 14. a) Frequency variations for both the MRF and the BF direction relevant to the whole experimental programme. Damping ratio box-plots are reported with whiskers referring to the 10^{th} and 90^{th}-quantile; b) mode shapes relevant to frequencies $f_n = 2.88 - 4.24 - 6.38 - 9.17 Hz$ of Table 7.

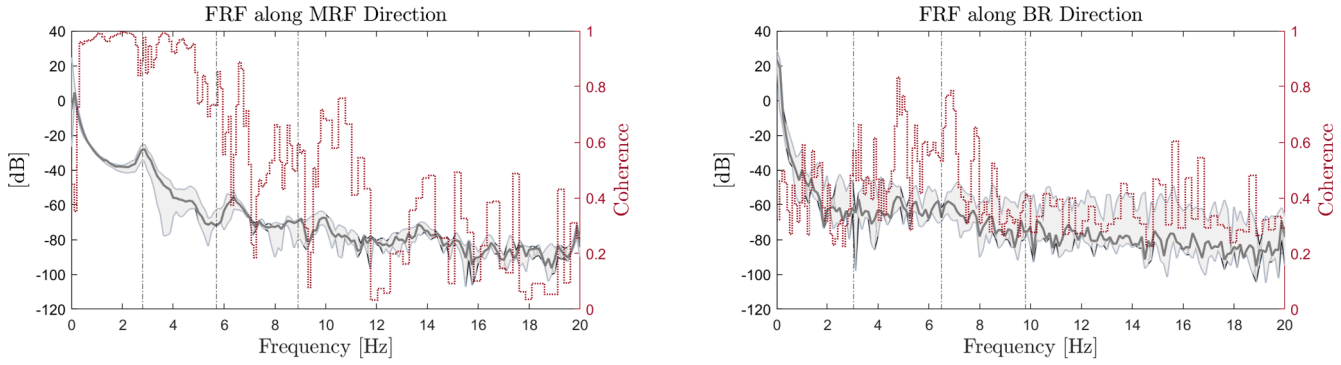
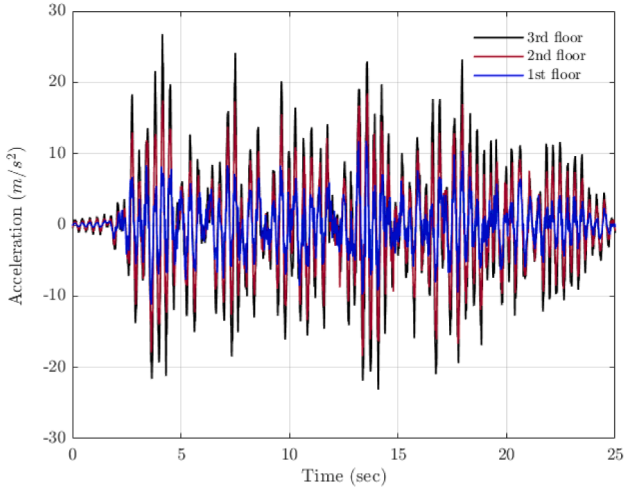
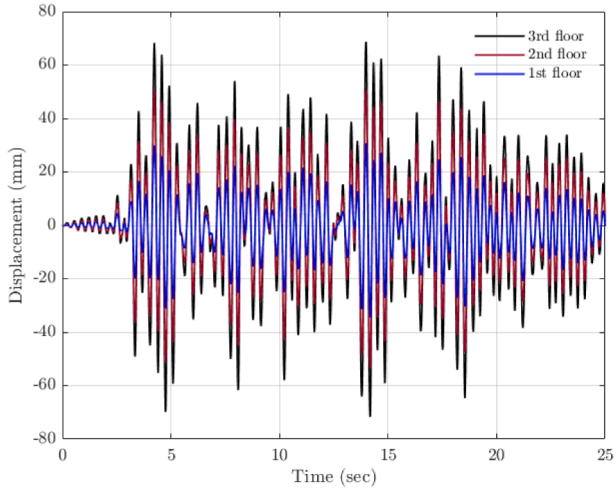


Fig. 15. Frequency response functions and coherence $C_{xy}(\omega)$ for the record TH #8–25% both for the MRF direction and the BF direction.

#4 for PGA level of 110%. The relative displacement is measured by the marker at the top of the vertical tanks and at the middle height of the horizontal ones. The results show that vertical tank on the first level exhibit almost four times higher displacements in comparison to the horizontal tank on the second level. Owing to significant rocking, we focused our attention on the vertical Tank #2 located in the first floor and depicted in Fig. 8b. It experienced a horizontal displacement of 19 mm along the MRF direction during the run T-H #8 110%. Although the Tank #2 exhibited significant rocking at this level of seismic excitation, limited damage was observed at the tank base. This experimental evidence confirms some statements of Section 1 about the over-conservatism of current standards for secondary elements, i.e. process equipment, in industrial facilities. Concerning the piping system, it is worth noticing the collapse of one suspended pipe system at the third floor, see Fig. 21, while performing the tuning phase of the record TH #8–37%. Furthermore, in order to evaluate both maximum values of flange opening and possible leakage detection, measures from SGs and LVDTs were recorded. Relevant maximum values are reported in Table 8. Measured values entail no leakage or LoC at flanged joints; moreover, standard pressure transducers confirm this conclusion. In addition, the conveyor located at the base suffered damage, see Fig. 20, due to failure of the bracing system as indicated in Fig. 20. Fig. 24a shows the acceleration time history of the cabinet for the record TH #8–110%. The cabinet and the connection remained undamaged as the mass of 140 kg is relatively low. The cabinet experienced 26.5 m/s^2, higher than the accelerations of the tanks on first floor, as the cabinet exhibits a high stiffness and low damping values. The dominant frequency at the highest amplitude defines the dominant frequency of the



(a) Time history vs. acceleration



(b) Time history vs. displacement

Fig. 16. Accelerations and displacements recorded at the three floor levels for the seismic record TH #8–110%.

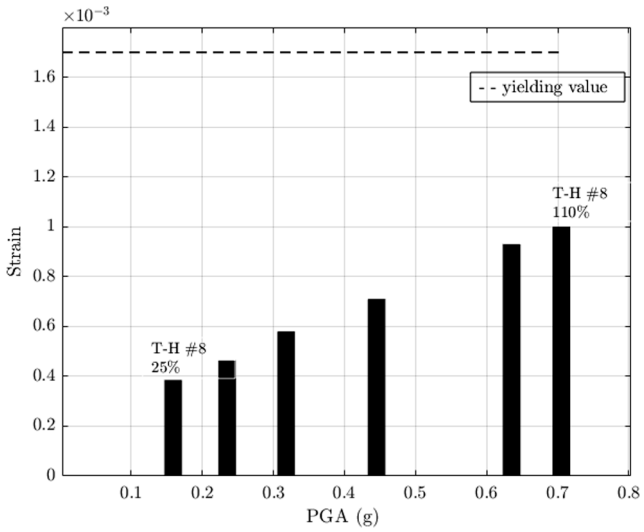


Fig. 17. Strain values of base columns vs. PGA recorded by strain gauges for different seismic records.

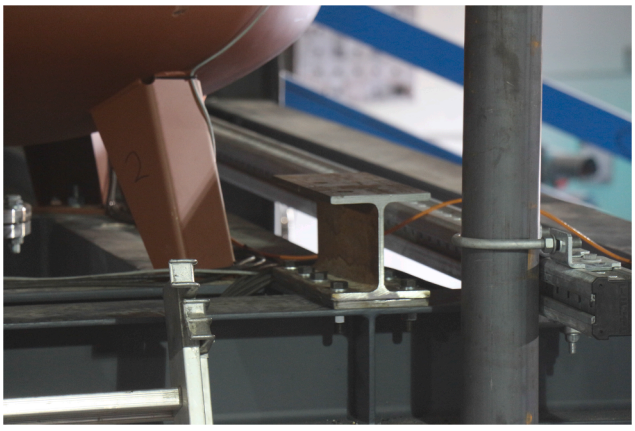


Fig. 18. Additional bolted tee stub used to connect the crossbeam to the main beam.

floor of 2.88 Hz, which corresponds to the first eigenfrequency of the primary structure. Moreover, eigenfrequencies in the range of 4.7 to 6 Hz shown in Fig. 24 correspond to the relevant frequencies of the overall system.

5. Data Analysis and Insights

The test results presented in SubSection 4.2 are analyzed in depth herein, completing observations provided in SubSection 1.1.

5.1. Floor responses and comparisons with literature and standards

It is worthwhile to underline that the dynamic interaction between primary structure and process equipment cannot be ignored in seismic analysis when designing process or secondary elements. In this respect, EN-1998 [12] does not provide any criterion to identify thresholds for which dynamic interaction can be neglected, ASCE 7–16 adopts the so-called 25% mass rule [27]. In the present scenario, this rule is clearly not satisfied and, thus, dynamic interaction between primary and secondary components should be explicitly accounted for. Moreover, according to Merino et al. [7] the use of EN-1998 [12] is rather conservative. In order to analyze this issue in depth, FRS at first and second floor have been directly derived by experimental data. In this respect, the signals recorded by accelerometers at the base of Tank #1 and #3 located at the first and the second floor, see Fig. 8, for two different time histories, i.e. TH #8–50% -PGA = 0.31 g- and TH #8–110% -PGA 0.71 g-, were used. Floor acceleration spectra for each of the three floors and a damping ratio of $\xi = 4.5\%$ are depicted in Fig. 25, where the damping value derives from experimental data treated in SubSection 4.1. A careful reader can notice that the dominant frequency is quite close to the natural frequency of the steel support structure, i.e. 0.34 s from Table 5, which does not change both with floor and PGA level. With regard to the amplitude, the high spectral values at the first floor, i.e.$1.5m/sec^2$ denote a predominant linear behaviour of the primary structure. Besides EN1998–1 [12] and ASCE 7–16 [27], several authors proposed refined approaches for the prediction of FRS. In this respect, it is worthwhile to recall the methods proposed by Calvi and Sullivan [52] and Vukobratovic and Fajfar [53]. In particular, the first approach is based on a dynamic amplification coefficient for secondary components as a function of the primary/secondary period ratio and the damping ratio of non-structural components. The authors also accounted for the nonlinear behaviour of the primary structure by using an equivalent period as a function of the kinematic ductility. The second approach instead, combines spectral accelerations of the primary and secondary



(a) Cracking and warping of fin plate FP #1 during TH #8-70%

(b) Damages of fin plate FP #2 during TH #8-100%

(c) Cracks and warping of fin plate FP #2 during TH #8-110%

Fig. 19. Cracks and warping of fin plate connections between primary MRF beam and secondary crossbeams at the first floor.



Fig. 20. Collapse of the supporting system of the conveyor at base level for record TH #8–110%.

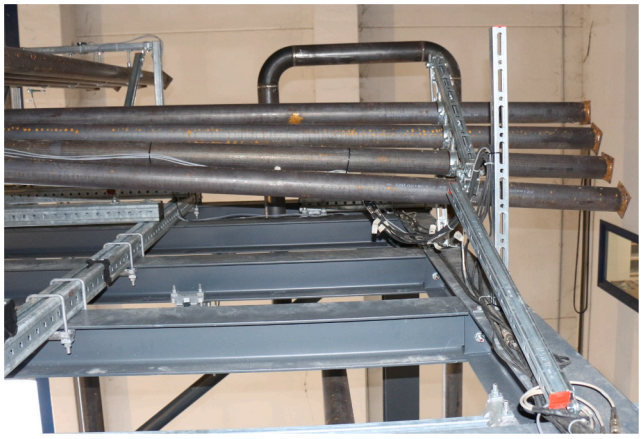
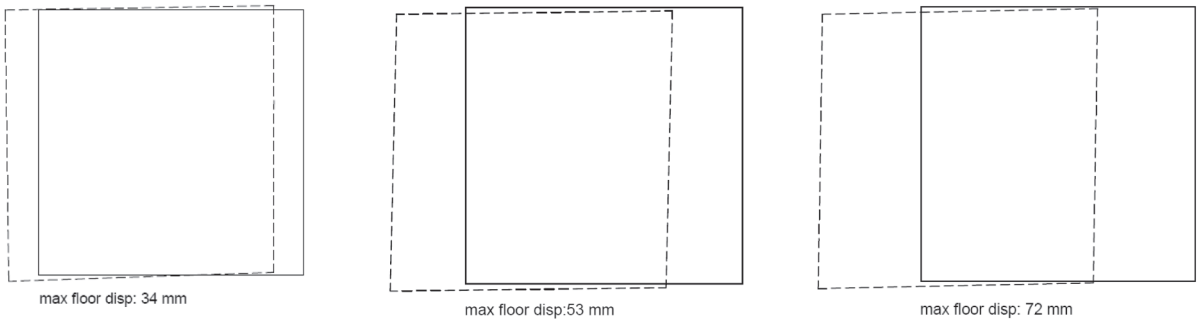


Fig. 21. Collapse of the pipe rack at the third floor.

system subjected to the ground acceleration by means of the well-known SRSS rule. Moreover, this method can account for the nonlinear behaviour of the primary structure. In addition, an importance factor $I_p = 1.5$ was used for ASCE 7–16 with a response modification factor $R_p = 2.5$ and a factor $q = 1.5$ for EN-1998. For the latter a component amplification factor equal to 2.5 has also been assumed. Relevant results are depicted in Fig. 26 and the reader can observe a general underestimation of amplitude values at resonance conditions for both EN-1998 and ASCE 7–16 standards, in line with the findings of [7]. Conversely, the good prediction capability at resonance of the method proposed by [52] is clearly confirmed. Nonetheless, one can deduce from Table 9, where both Tank #1 and #3 are considered, that the aforementioned method cannot accurately predict the FRS ordinate at the natural frequency of tanks. Differently, the method proposed by [53] appears more reliable in both the prediction of spectral shape, see Fig. 25, and the estimation of floor spectral accelerations relative to tanks, i.e. Table 9. Also in this case, a ductility value of 1.5 has been assumed to be consistent with the standard EN-1998–1. Design rules offered by the European [12] and American standards [27] for secondary elements have been widely discussed in literature [54,40]. More precisely, it was demonstrated that the prediction capacity of code-compliant formulations appear rather limited. For instance, Merino et al. [7], observed that in case of storage tanks, the EN-1998 approach wrongly estimates acceleration demands over a wide range of vibration periods. A general underestimation close to the resonance condition is also observed; whereas a significant overestimation is present in other period ranges. Similar under/over estimations have been observed with the application of ASCE 7–16, where the dependency from the secondary/primary period ratio is not included. The main reasons behind the inaccurate estimation of both codes are related to: i) the absence of damping ratio for floor spectra estimation; ii) a general overestimation of the behaviour factor [55] and the component response modification factor for secondary elements. These considerations are reflected in the acceleration value predictions of Table 9 where all floor accelerations were evaluated at the fundamental period of Tank #1–0.11 s - and Tank #3–0.08 s -, respectively. The overconservatism of predicted code values is evident.

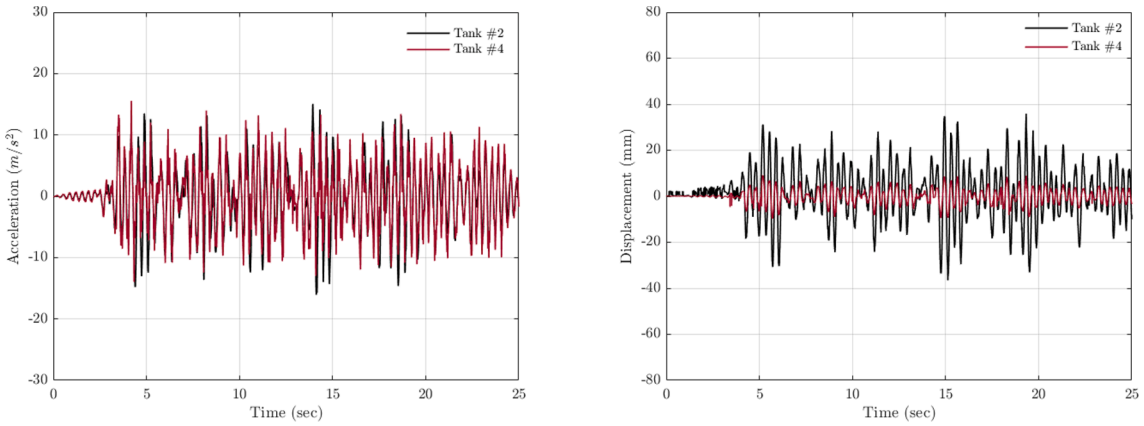
5.2. Structural regularity considerations

As far as in plan regularity is concerned, current standard [12,27] classify the primary structure as irregular because of the absence of rigid floors. This feature can also be investigated from the analysis of both acceleration and displacement profiles of the primary structure, as illustrated in Fig. 27a and 27b. The distribution of the kinematic responses along the height for increasing seismic intensity, clearly demonstrates a regularity, even in the absence of rigid floors and with unequal mass distribution. As a result any damage concentration can be excluded. The exception is only represented by the case characterized by the seismic record TH #8–100%. The reason is probably due to the local damage occurred during the previous test, i.e. due to the record TH #8-70%. As already observed in SubSection 4.2, during the seismic response, a relevant sectional rotation of the crossbeam under vertical Tank #2 located at the first floor, caused connection web warping and



(a) First floor (marker #20) (b) Second floor (marker #46) (c) Third floor (marker #65)

Fig. 22. Floors motion recorded by means of marker sensors for the record TH #8–110%.



(a) (b)

Fig. 23. Comparison of time histories for Tank #2 and Tank #4 subjected to the record TH #8–110%: a) acceleration; b) relative displacement.

Table 8
Piping system w.r.t. Fig. 9 and response.

Pipe position	Max Strain (‰)	Max opening (mm)
# 1	0.3	0.02
# 4	0.1	0.03
# 5	0.4	0.03
# 6	0.2	0.051

generated important cracks, as depicted in Fig. 19. Eventually, we can argue that the structure exhibited a general regular behaviour during testing.

Along this vein, in order to study the acceleration profile and the amplification factors, also the structural regularity of secondary elements like tanks, has been investigated. In this respect, Fig. 28, depicts the peak acceleration both at the base and at the top of the vertical Tank #2 and the horizontal Tank #3, see Fig. 8, for each run of the test programme. The top acceleration increase appears rather linear with the PGA level growth and the amplification of the base acceleration is almost constant for each run, except for the run TH #8-70%, where

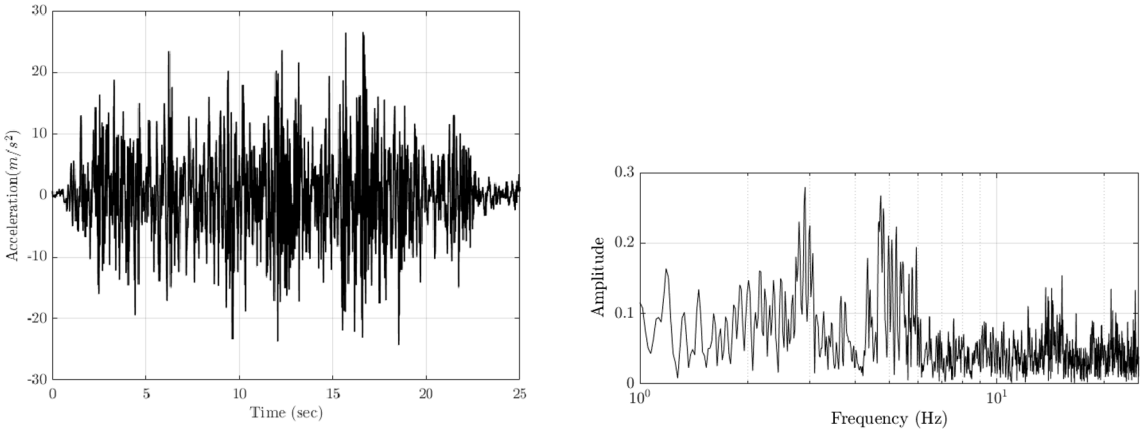
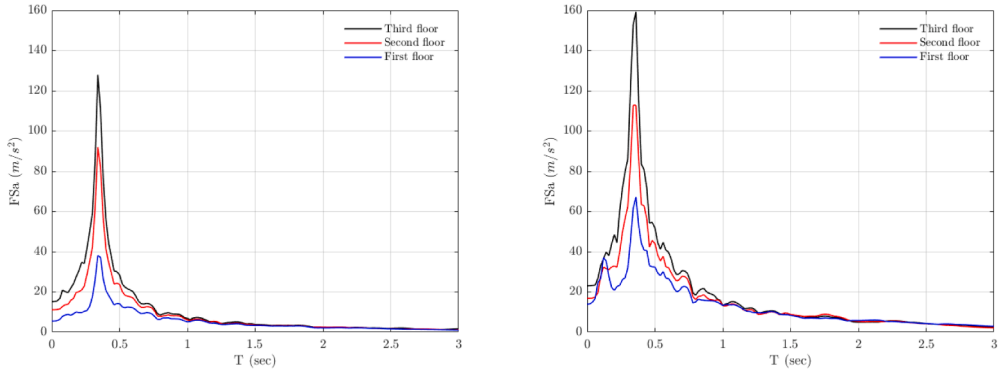
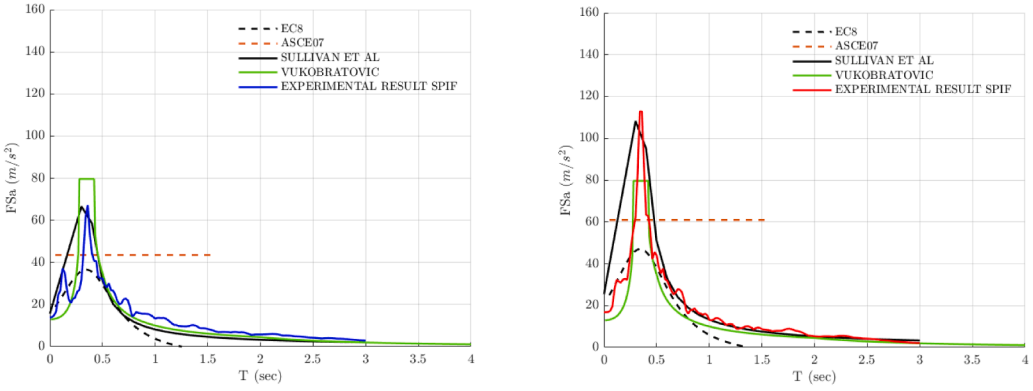


Fig. 24. (a) Acceleration time history of the sensor A #13 of the cabinet at Level 1 for the record TH #8–110% and (b) relevant frequency spectrum.



(a) Record TH #8-50% (b) Record TH #8-110%

Fig. 25. Experimental floor response spectra for TH #8–50% and TH #8–110% seismic excitations.



(a) First floor spectra for the Record TH #8-110% (b) Second floor spectra for the Record TH #8-110%

Fig. 26. Comparison between analytical and experimental floor response spectra for the Record TH #8–110%.

Table 9
Comparison of floor response spectra ordinates at the fundamental period of Tanks #1 and #3.

PGA	Tank	Experimental	FRS	EN 1998–1	ASCE- 7	Sullivan	Vukobratovic
(g)	#	acceleration (m/s^2)	acceleration (m/s^2)	acceleration (m/s^2)	acceleration (m/s^2)	et al. (m/s^2)	and Fajfar (m/s^2)
0.31	1	7.68	10.96	10	20	22	7
	3	12.82	14.31	27	27	40	13
0.71	1	15.06	30.10	22	43	32	14
	3	18.48	25.10	25	60	53	17

damage of the crossbeam occurred. We can argue that the linear behaviour of the secondary elements agrees with that of the main structure.

6. Conclusions and future developments

The SPIF project -Seismic Performance of Multi-Component Systems in Special Risk Industrial Facilities- was proposed within the framework of the European H2020 - SERA (Seismology and Earthquake Engineering Research Infrastructure Alliance for Europe) funding scheme -. It focuses on the investigation of the seismic behavior of a representative industrial moment resisting frame substructure equipped with process secondary components by means of shaking table tests. The test campaign was comprehensive and carried out at the EUCENTRE Laboratory of Pavia, Italy. A full scale mock-up composed by two single-bay moment resisting frames with three floors, total height 9.3 m, was built and tested using a unidirectional shaking table with several earthquake levels. In this respect, a spectrum-compatible record, based on a EN-1998–1 [12] spectrum was selected. The testing campaign demonstrated a dynamic interaction between the primary steel structure and secondary process units that clearly influenced the performance of the whole system. More precisely, the primary steel structure remained undamaged also for SSE earthquake levels mainly due to its design and inherent flexibility that avoided a strong interaction with secondary components. Some damage instead, appeared in web plates of supported crossbeams in the area of fin plate connections between main members and secondary beams; that happened due to the interaction between primary and secondary components, that justified a light seismic retrofit intervention in that area by means of a bolted tee stub. Moreover, results clearly showed a general overconservatism of current design standards with respect to floor response spectra prediction of process units evaluated at their fundamental period, due to the lack of consideration of damping and overestimation of behaviour/reduction factors.

Overall, it was shown that a proper experimental test campaign can highlight complex interactions and potential damage locations present in industrial plant substructures. The efficiency of other steel

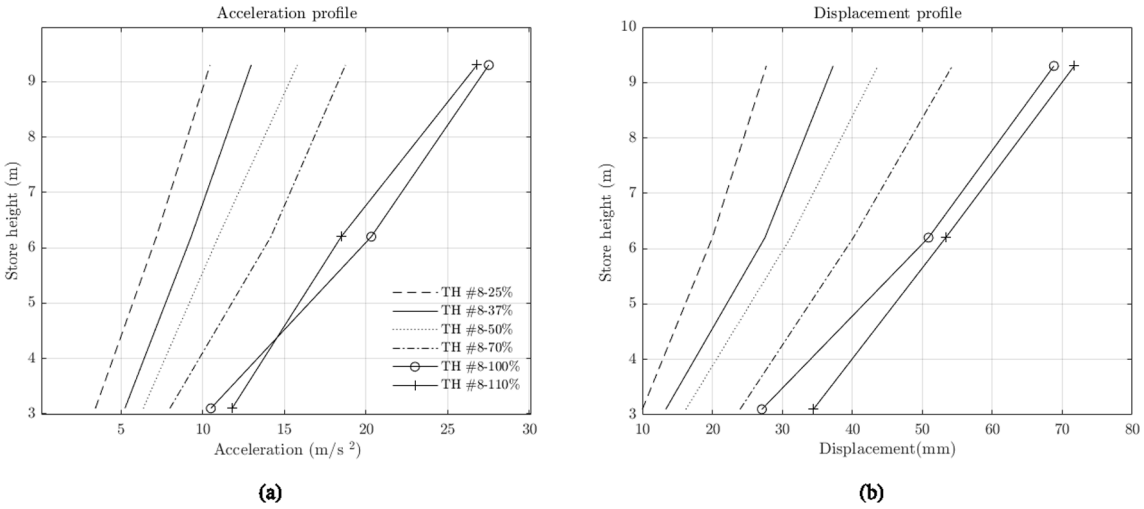
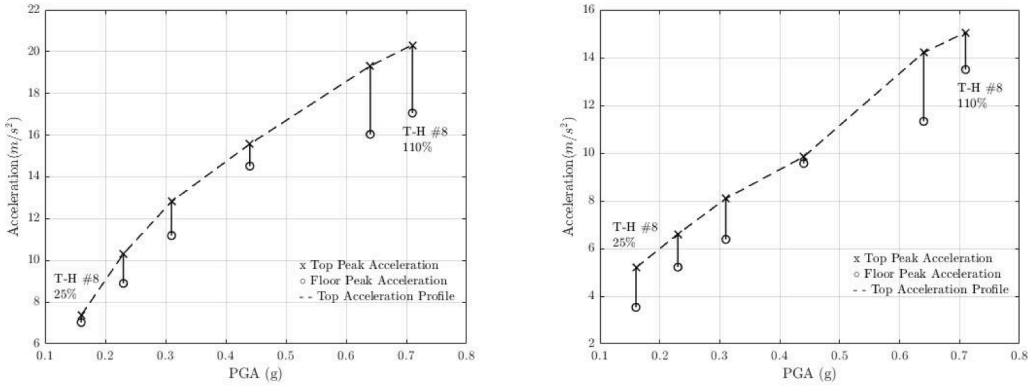


Fig. 27. Acceleration and displacement profiles for different THs.



(a) Vertical Tank #2 (b) Horizontal Tank #3

Fig. 28. Acceleration profiles of Tank #2 and Tank #3 for different PGA levels of TH #8.

configurations, e.g. a braced frame configuration, also in view of proper seismic retrofit interventions deserves further studies.

Declaration of Competing Interest

The authors declare that they have no known competing financial interests or personal relationships that could have appeared to influence the work reported in this paper.

Acknowledgements

The research leading to these results has received funding from the European Community's HORIZON 2020 Framework Programme [H2020-INFRAIA-2016–2017/H2020-INFRAIA-2016–1] for access to EUCENTRE Laboratory under grant agreement n° 730900-SERA project and from the Italian Ministry of Education, University and Research (MIUR) in the frame of the 'Departments of Excellence'(grant L 232/2016).

References

[1] Krausmann E, Renni E, Campedel M, Cozzani V. Industrial accidents triggered by earthquakes, floods and lightning: Lessons learned from a database analysis. Nat. Hazards 2011;59(1):285–300. https://doi.org/10.1007/s11069-011-9754-3.
[2] M. Erdik, E. Uckan, Earthquake damage and fragilities of industrial facilities, International Conference on Seismic Design of Industrial Facilities. (SEDIF 2013. doi:10.1007/s11069-011-9754-3.
[3] Cruz E, Valdivia D. Performance of industrial facilities in the chilean earthquake of 27 february 2010. The Structural Design of Tall and Special Buildings 2011;20:83–101.
[4] M. Campedel, Analysis of major industrial accidents triggered by natural events reported in the principal available chemical accident databases, Tech. rep., JRC42281, Joint Research Centre Institute for the Protection and Security of the Citizen, Ispra, Italy, report EUR 23391 EN - 2008 (2008).
[5] S.W. Swan, D.D. Miller, P.I. Yanev, Morgan hill earthquake of april 24, 1984 - effects on industrial facilities, buildings and other facilities., Earthquake Spectra 1 (3) (1985) 457–568. doi:10.1193/1.1585276.
[6] Suzuki K. Report on damage to industrial facilities in the 1999 kocaeli earthquake, turkey. J. Earthquake Eng. 2002;6(2):275–96. https://doi.org/10.1080/13632460209350417.
[7] R.J. Merino Vela, E. Brunesi, R. Nascimbene, Derivation of floor acceleration spectra for an industrial liquid tank supporting structure with braced frame systems, Engineering Structures. (vol. 171, pp. 105–122, 2018).
[8] De Biasio M, Grange S, Dufour F, Allain F, Petre-Lazar I. Intensity measures for probabilistic assessment of non-structural components acceleration demand. Earthquake Engineering & Structural Dynamics 2015;44(13):2261–80. https://doi.org/10.1002/eqe.2582.
[9] Kothari P, Parulekar Y, Reddy G, Gopalakrishnan N. In-structure response spectra considering nonlinearity of rcc structures: Experiments and analysis. Nucl. Eng. Des. 2017;322:379–96. https://doi.org/10.1016/j.nucengdes.2017.07.009.
[10] Filiatrault A, Christopoulos C, Stearns C. Guidelines, specifications and seismic performance characterization of nonstructural building components and equipment, PEER Report 2002/05. Berkeley, CA: University of California; 2001.
[11] Calvi P, Sullivan TJ, Nascimbene R. Towards improved floor spectra estimates for seismic design. Earthquake and Structures 2013;4:109–32.
[12] European Committee for Standardization, Design of structures for earthquake resistance. Eurocode 8-1, CEN/TC 250, Brussels, (2004).
[13] VCI-guideline: Guideline, seismic design in process industry, German Chemical Industry Association (October 2013).
[14] American Society of Mechanical Engineers, Power piping, ASME B31.1 standard, Washington DC, (2012).

[15] American Society of Mechanical Engineers, Process piping, ASME B31.3 standard, Washington DC, (2012).
[16] European Committee for Standardization. Metallic industrial piping – part 3: Design and calculation, EN 13480–3. Brussels: CEN; 2011.
[17] Task Committee on Seismic Evaluation and Design of Petrochemical Facilities of ASCE, Guidelines for seismic evaluation and design of petrochemical facilities, American Society of Civil Engineers (2011).
[18] O.S. Bursi, M.S. Reza, G. Abbiati, F. Paolacci, Performance-based earthquake evaluation of a full-scale petrochemical piping system., Journal of Loss Prevention in the Process Industries 10–22. doi:https://doi.org/10.1016/j.jlp.2014.11.004.
[19] ASCE/SEI, Seismic Analysis of Safety-Related Nuclear Structures., Standard 4–16, 2016.
[20] A.C. Caputo, B. Kalemi, F. Paolacci, D. Corritore, Computing resilience of process plants under na-tech events: Methodology and application to sesmic loading scenarios., Reliability Engineering & System Safetydoi:https://doi.org/10.1016/j.ress.2019.106685.
[21] A. Necci, V. Cozzani, G. Spadoni, F. Khanb, Assessment of domino effect: State of the art and research needs., Reliability Engineering & System Safety 3–18. doi:https://doi.org/10.1016/j.ress.2015.05.017.
[22] A. Alessandri, A.C. Caputo, D. Corritore, R. Giannini, F. Paolacci, N. Phan, Probabilistic risk analysis of process plants under seismic loading based on monte carlo simulations., Journal of Loss Prevention in the Process Industries 136–148. doi:https://doi.org/10.1016/j.jlp.2017.12.013.
[23] G. Fabbrocino, I. Iervolino, F. Orlando, E. Salzano, Quantitative risk analysis of oil storage facilities in seismic areas., Journal of Hazardous Materials 61–69. doi:https://doi.org/10.1016/j.jhazmat.2005.04.015.
[24] Vathi M, Karamanos S, Kapogiannis I, Spiliopoulos K. Performance criteria for liquid storage tanks and piping systems subjected to seismic loading. Journal of pressure vessel technology 2017. https://doi.org/10.1115/1.4036916.
[25] Reza MS, Bursi OS, Paolacci F, Kumar A. Enhanced seismic performance of non-standard bolted flange joints for petrochemical piping systems. J. Loss Prev. Process Ind. 2014;30. https://doi.org/10.1016/j.jlp.2014.05.011.
[26] European Committee for Standardization, Silos, tanks and pipelines. eurocode 8-part 4, CEN/TC 250, EN 1998-4, Brussels, (2006).
[27] ASCE/SEI, Minimum Design Loads and Associated Criteria for Buildings and Other Structures., Standard 7–16, 2016.
[28] M. Okeilchi, C. Tung, Effects of ductility on seismic response of piping systems and their implication on design and qualification., Nuclear Engineering and Design 69–83. doi:https://doi.org/10.1016/0029-5493(96)01236-8.
[29] O. Bursi, F. Paolacci, M.S. Reza, S. Alessandri, N. Tondini, Seismic assessment of petrochemical piping systems using a performance-based approach, Journal of Pressure Vessel Technology 138 (06 2016). doi:10.1115/1.4032111.
[30] A. Maekawa, T. Takahashi, Numerical study on inelastic seismic design of piping systems using damping effect based on elastic–plastic property of pipe supports, Journal of Pressure Vessel Technology 1–9. doi:https://doi.org/10.1115/1.4039697.
[31] S. Kwag, Y.H. Ryu, B.S. Ju, Efficient seismic fragility analysis for large-scale piping system utilizing bayesian approach., Journal of Applied Sciences 61–69. doi:https://doi.org/10.3390/app10041515.
[32] G. Chock, T. Kindred, I. Robertson, G. Iinuma, P. Nicholson, E. Lau, H. Brandes, A. Sarwar, E. Medley, J. Pino, P. Okubo, W. Holmes, B. Hirshorn, J. Sumada, Compilation of observations of the october 15, 2006 kiholo bay (mw 6. 7) and mahukona (mw 6.0) earthquakes, hawaii, tech.rep. (12 2006).
[33] Mosqueda G, Retamales R, Filiatrault A, Reinhorn A. Testing facility for experimental evaluation of non-structural components under full-scale floor motions. The Structural Design of Tall and Special Buildings 2009;18(4):387–404. https://doi.org/10.1002/tal.441.
[34] Meskouris K, Butenweg C, Hinzen K-G, Höffer R. Structural dynamics with applications in earthquake and wind engineering. Springer Verlag; 2019.
[35] O. Bursi, R. di Filippo, Component fragility evaluation, seismic safety assessment and design of petrochemical plants under design-basis and beyond-design-basis accident conditions, Tech. rep., Final Report, INDUSE-2-SAFETY Project, Contr. No: RFS-PR-13056, Research Fund for Coal and Steel (2018).
[36] F. Paolacci, M.S. Reza, O. Bursi, Seismic analysis and component design of refinery piping systems., COMPDYN 2011 -III ECCOMAS Thematic Conference on Computational Methods in Structural Dynamics and Earthquake Engineering, (Corfu, Greece, 26–28 May 2011).
[37] U.S.NRC, Seismic analysis of large-scale piping systems for the jnes-nupec ultimate strength piping test program, Office of Nuclear Regulatory Research (2008).
[38] U.S. Department of Energy, Seismic evaluation procedure for equipment in u.s. deparment of energy facilities, Office of Defense Programs and Office of Environment, Safety and Health (1997).
[39] Wang Z, Pedroni N, Zentner I, Zio E. Seismic fragility analysis with artificial neural networks: Application to nuclear power plant equipment. Eng. Struct. 2018;162:213–25. https://doi.org/10.1016/j.engstruct.2018.02.024. http://www.sciencedirect.com/science/article/pii/S0141029617326858.
[40] Di Sarno L, Karagiannakis G. Petrochemical steel pipe rack: Critical assessment of existing design code provisions and a case study. International Journal of Steel Structures 2020:232–46. https://doi.org/10.1007/s13296-019-00280.
[41] O. Azizpour, M. Hosseini, A verification study of asce recommended guidlines for seismic evaluation and design of combination structures in petrochemical facilities., Journal of Applied Sciences 3609–3628.
[42] Ezeberry J, Combescure D. A direct method for determining floor response spectra at the iter tokamak complex. Nucl. Eng. Des. 2017;323:290–8. https://doi.org/10.1016/j.nucengdes.2017.01.030.
[43] C. Butenweg, al. et., Seismic performance of multi-component systems in special risk industrial facilities, Tech. rep., Deliverable D10.1, SERA Project, Project. No: 730900, H2020-EU – Seismology and Earthquake Engineering Research Infrastructure Alliance for Europe (2020).
[44] Cornell C, Krawinkler H. Progress and challenges in seismic performance assessment. PEER Center News 2000;3.
[45] Norme Tecniche per le costruzioni, DM 18 Gennaio 2018, Norme Tecniche, 2018.
[46] Differences in approach between nuclear and conventional seismic standards with regard to hazard definition., CSNI Integrity and Ageing Working Group, Nuclear Energy Agency Committee on the Safety of Nuclear Installations.
[47] E. Chatzi, C. Papadimitriou, Identification Methods for Structural Health Monitoring, Springer, 2016. doi:10.1007/978-3-319-32077-9.
[48] Richardson MH, Formenti DL. Parameter Estimation From Frequency Response Measurements Using Rational Fraction Polynomials. In: Proceedings of the International Modal Analysis Conference & Exhibit; 1982. p. 167–81.
[49] R. Brincker, C. Ventura, Introduction to Operational Modal Analysis, WILEY, 2015.
[50] C. Rainieri, G. Fabbrocino, Operational Modal Analysis of Civil Engineering Structures - An Introduction and Guide for Applications., Springer, 2014.
[51] Friswell M, Mottershead J. Finite element model updating in structural dynamics. Tech. rep. Kluwer Academic Publishers; 1994.
[52] Calvi P, Sullivan TJ. Estimating floor spectra in multiple degree of freedom systems. Earthquake and Structures 2014;7:17–38. https://doi.org/10.12989/eas.2014.7.1.017.
[53] Vukobratovic V, Fajfar P. A method for the direct estimation of floor acceleration spectra for elastic and inelastic MDOF structures. Earthquake Engineering Structural Dynamic 2016;45:2495–511.
[54] Petrone CJ, Magliuolo G, Manfredi G. Floor response spectra in rc frame structures designed according to eurocode 8. Bull Earthquake Eng 2015;2016(14):747–67. https://doi.org/10.1007/s10518-015-9846-7.
[55] Giannini R, Paolacci F, De Angelis M. Experimental investigation on the seismic response of a steel liquid storage tank equipped with floating roof by shaking table tests. Earthquake Engineering Structural Dynamic 2010;39:377–96. https://doi.org/10.1002/eqe.945.